Thesis for the degree of Licentiate of Engineering

Conceptual design of the hydrogen-enhanced intercooler

Petter Miltén

Department of Mechanics and Maritime Sciences
CHALMERS UNIVERSITY OF TECHNOLOGY
Gothenburg, Sweden 2025

Conceptual design of the hydrogen-enhanced intercooler
Petter Miltén

© Petter Miltén, 2025.

Licentiatavhandlingar vid Chalmers tekniska högskola

Department of Mechanics and Maritime Sciences
Chalmers University of Technology
SE–412 96 Göteborg, Sweden
Telephone + 46 (0) 31 – 772 1000

Chalmers Reproservice
Göteborg, Sweden 2025

To my unborn son

Abstract

Conceptual design of the hydrogen-enhanced intercooler
Petter Miltén
Department of Mechanics and Maritime Sciences
Division of Fluid Dynamics
Chalmers University of Technology

Previous research has shown that intercooling is a key enabler for allowing the introduction of future engine concepts with high thermal management demands. One such engine concept is the composite cycle engine (CCE), which combines the high power density of the turbomachinery with the increased thermal efficiency of an internal combustion engine (ICE). Implementing intercooling, where fan discharge air is used as coolant, into the CCE has shown a potential reduction of 20% in the weight of the ICE! Further, using hydrogen as an aircraft fuel, stored in cryogenic state, improves the benefits from intercooling when used as a coolant. Although the low fuel mass flow, hydrogen can facilitate substantial cooling of the core-air stream because of the very low storage temperatures and outstanding thermal properties. The EU project MINIMAL was formed to further develop the intercooled CCE fuelled by hydrogen. The required cooling is expected to exceed the possible values if using only the fan discharge air or the fuel. Hence, the aim of this thesis will be to investigate the hydrogen-enhanced intercooling concept, where the idea is to use both the fan discharge air and hydrogen for intercooling.

The first phase in developing the hydrogen-enhanced intercooler is to facilitate easy heat exchanger design space exploration. A novel method (GenHEX) is developed which generalizes the heat exchanger matrix geometry down to three geometrical generalization parameters (GGPs). This enables a design approach that reduces the demands on designer intuition, luck, and access to extensive databases. Instead, it uses correlations for estimating the aerothermal performance and an application specific objective function to decide the best combination of GGPs, which then guides the designer in designing the heat exchanger. This novel method is the basis for Paper 1, where it was validated against state-of-the-art heat exchanger performance.

The second phase discusses the down-selection of various hydrogen-enhanced intercooler arrangements and important design considerations such as the risk of freezing, hydrogen leakage, and structural integrity. Semi-idealized heat exchangers were used for the down-selection, and one arrangement was selected for further investigation using the GenHEX method to estimate the performance with and without design constraints for risk mitigation. The findings during the second phase are the basis for Paper 2.

Keywords: intercooling, heat exchangers, hydrogen, freezing, conceptual design

Acknowledgments

First and foremost I would like to thank my supervisors Carlos Xisto, Isak Jonsson and Anders Lundbladh. Without Carlos's exceptional attention to details, Isak's phenomenal intuition, and Anders's remarkable breadth of knowledge, I would not be standing here feeling this proud of my work. Your hard work and devotion encourage me to strive for perfection. I also would like to thank my examiner Tomas Grönstedt and unofficial supervisors Xin Zhao and Alexandre Capitao Patrao, who laid the foundation on which I have built upon and are always available for discussions when I feel lost. Furthermore, I would like to thank all the colleagues and staff at the Department of Mechanics and Maritime Sciences, Division of Fluid Dynamics, at Chalmers University of Technology. Together, I believe that we could actually make the world a better place. Next, I want to acknowledge project MINIMAL which is co-funded by the European Union's Horizon Europe Programme under the grant agreement n°101056863. Thanks for funding my research.

A special thanks goes out to my work-life family with whom I share the turbo-room. Emil Ellenius and Filip Herbertsson are the latest additions, I look forward to getting to know you better and I wholeheartedly believe that one day you will outclass us all. Adam Johansson, thanks for being bright enough to light up the darkest of days and warmhearted enough for everyone in your presence to feel comfortable. It is truly rare to meet someone who knows exactly what words of encouragement are needed to lift me up. Carl Larsson, although you are far away on the other side of the building, I know that I can always count on you and ever since we spent those countless nights together in the basement during out formula year, your presence in my life has felt obvious. Christian Svensson, we have been sidekicks for almost 5 years now throughout multiple years in Chalmers Formula Student, our joint master thesis and our first years as researchers. I am not tired of you and the privilege is mine! Thank you for always listening to my brain farts and every moment I have spent in your presence has enriched my life, whether it has been burgers at JA or slapping you with lingongrova.

To all those who feel included as my friends, thank you for encouraging me to spend time doing other things than work. Whether it is late night running in the rain, house renovations, board games, celebrating kräftdröm, or lunches in Stockholm.

Last but most importantly, I want to express my deepest gratitude to my extended family. My mother Christina, father Peter, brother Pontus, his girlfriend Carro and my relatives in Uddevalla and elsewhere. Words are not enough, but thank you for your endless support in all aspects of life! To my loving fiancee and unborn son, you mean the world to me and there is nothing I would not do for you.

Petter Miltén
Gothenburg, January 2025

List of Publications

This thesis is based on the following appended papers:

Paper 1. Petter Miltén, Isak Jonsson, Anders Lundbladh and Carlos Xisto. *GENERALIZED METHOD FOR THE CONCEPTUAL DESIGN OF COMPACT HEAT EXCHANGERS*. J. Eng. Gas Turbines Power. Nov 2024, 146(11) https://doi.org/10.1115/1.4065922

Paper 2. (Submitted manuscript) Petter Miltén, Isak Jonsson, Anders Lundbladh and Carlos Xisto.
CONCEPTUAL DESIGN EXPLORATION OF HYDROGEN ENHANCED INTERCOOLING FOR FUTURE AEROENGINES. ASME 2025 Turbomachinery Technical Conference & Exposition, June 2025, Memphis, Tennessee USA

Other publications

The following relevant publications are authored or co-authored by Petter Milté. However, they are not appended to, or part of, this thesis:

Paper I. VT Silva, A Lundbladh, C Xisto, P Miltén, I Jonsson.
Powered Low-Speed Experimental Aerodynamic Investigation of an Over-Wing-Mounted Nacelle Configuration. J. Aircraft. Mar 2024, 61(2)
https://doi.org/10.2514/1.C037653

Paper II. I Jonsson, A Capitao Patrao, P Miltén, C Xisto, M Lejon.
Experimental and Numerical Study on the Effect of OGV Clocking on ICD Performance. Turbo Expo: Power for Land, Sea, and Air. June 2024, London England
https://doi.org/10.1115/GT2024-123733

Paper III. C Svensson, P Miltén, T Grönstedt
MODELLING HYDROGEN FUEL CELL AIRCRAFT IN SUAVE. 34th ICAS Congress. June 2024, Florence Italy

Paper IIII. A Johansson, P Miltén, A Lundbladh, C Xisto
MODELLING A HYDROGEN FUELLED COMPOSITE CYCLE AERO-ENGINE. 34th ICAS Congress. June 2024, Florence Italy

Nomenclature

Acronyms

CCE	–	Composite Cycle Engine
ENABLEH2	–	ENABLing cryogEnic Hydrogen based CO2 free air transport
EU	–	European Union
FAR	–	Fuel-to-Air Ratio
GGP	–	Geometrical Generalization Parameters
HEX	–	Heat EXchanger
IC	–	InterCooler
ICE	–	Internal Combusion Engine
LEMCOTECH	–	Low Emissions Core-Engine Technologies
MINIMAL	–	MInimum enviroNmental IMpact ultra-efficient cores for Aircraft propuLsion
NEWAC	–	NEW Aero engine Core concepts
ULTIMATE	–	Ultra Low emission Technology Innovations for Mid-century Aircraft Turbine Engines

Latin Letters

A	–	Area [m^2]
C	–	Heat capacity rate [W K^{-1}]
c_p	–	Specific heat capacity [J kg^{-1} K^{-1}]
D_h	–	Hydraulic diameter [m]
h	–	Heat transfer coefficient [[Wm^{-2} K^{-1}]
H_2	–	Hydrogen
k	–	Thermal conductivity [Wm^{-1} K^{-1}]
ℓ	–	Undisturbed flow length [m]
L	–	Length [m]
m	–	Fin effectiveness parameter [m^{-1}]
$\dot{m}$	–	Mass flow [kg s^{-1}]
p	–	Pressure [Pa]
Q	–	Cooling power [W]
t	–	Thickness [m]
T	–	Temperature [K]
u	–	Flow velocity [m s^{-1}]
V	–	Volume [m^3]

Non Dimensional Number

Re	–	Reynolds number
Γ	–	Coefficient of performance
ε	–	Effectiveness
f	–	Friction factor
η_p	–	Polytropic efficiency
j	–	Colburn factor
Nu	–	Nusselt number
Pr	–	Prandtl number

Greek Symbols

α	–	Surface area density [m^{-1}]
δ	–	Boundary layer height [m]
Δ	–	Difference in
Π	–	Pressure ratio
ρ	–	Density [kg m^{-3}]
σ	–	Void fraction
Φ	–	Specific power [W kg^{-1}]
χ	–	Solid-volume to total-volume fraction

Subscripts

c	–	local
f	–	finned
ff	–	free-flow
fr	–	frontal
ftt	–	finned to total
in	–	inlet
m	–	mean
out	–	outlet
r	–	ratio
s	–	solid
t	–	total
w	–	wetted
W	–	Wall
wf	–	wetted fin
x	–	local

Contents

Part I

Introductory Chapters

Chapter 1

Introduction

1.1 Background

The transportation sectors contributed to a quarter of the EU's total CO_2 emissions in 2019, out of which 13.4% were attributed to civil aviation. Road transportation was the main contributor, accounting for 71.7% [1]. However, battery electric mobility is especially suitable for the road transportation sector, where it is expected to substantially reduce CO_2 emissions. In contrast, an equivalent solution for the aviation sector has yet to be found. Hence, the fraction of total emissions attributed to aviation is expected to increase.

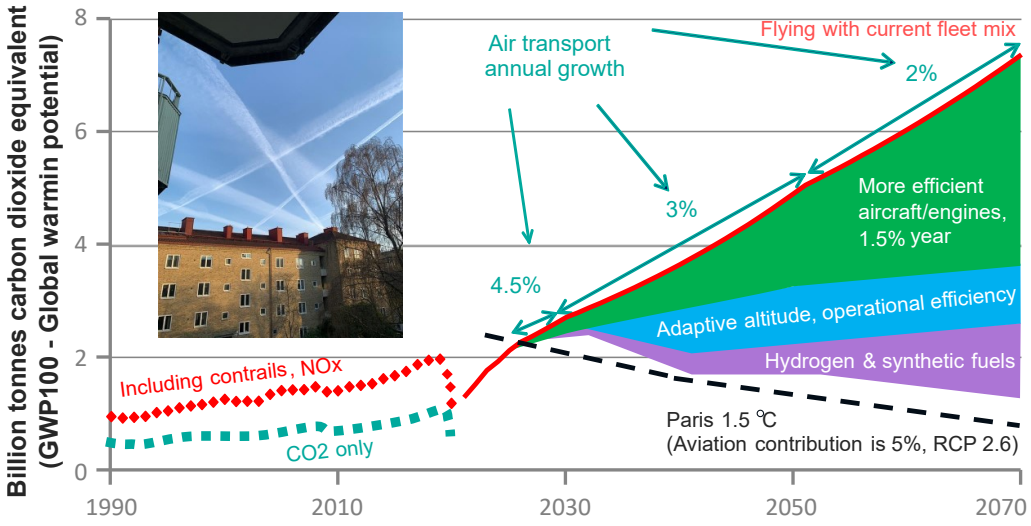

Figure 1.1: Evolution of the carbon dioxide equivalent global warming potential from the civil aviation sector. Courtesy: Anders Lundbladh GKN Aerospace

Figure 1.1 illustrates the increase in emissions from the civil aviation sector if the current fleet mix is maintained. The figure also shows the potential reductions from the increased efficiency of aircraft and engine efficiency, improved operational efficiency, and the introduction of hydrogen and synthetic fuels. The figure shows that although aircraft and their engines are becoming more efficient, not even an aspirational goal of 1.5% per year would be enough to counter the annual growth

in air transport (2 to 4.5%), leading to a net increase in emissions. It also shows that CO_2 emissions alone are not enough to account for the entire climate impact from the aviation sector. Other short-lived climate-forcing emissions, including contrails, NOx, water vapor, aerosols, and soot, also contribute significantly. The two main contributors to these non-CO_2 emissions are contrails and NOx, and their CO_2 equivalent impacts are shown as red squares in 1.1, along with a photograph of contrails covering a large fraction of the sky above Guldheden in Gothenburg. Contrail formation can be reduced by altering flight paths and altitudes to avoid regions with critical humidity and temperature levels. Even with all the above mitigation methods, meeting the targets set at the 2019 UN Climate Action Summit in Paris, limiting the global temperature increases at the end of the century to a maximum of 1.5 °C, will be challenging. There are large uncertainties regarding the impact from non-CO_2 emissions, but contrails and NOx are estimated to contribute to about 66% of the net aviation radiative forcing [2]. Project MINIMAL (MInimum enviroNmental IMpact ultra-efficient cores for Aircraft propuLsion) [3] was founded to further increase the knowledge regarding these non-CO_2 emissions and investigate the potential reduction of net radiative forcing by introducing new aero-engine core technology and alternative fuels. This approach has the potential to reduce the impact from contrails by 80%, NOx by 52%, and CO_2 by 36% (if using conventional Jet-A fuel) relative to 2020, as illustrated in Figure 1.2.

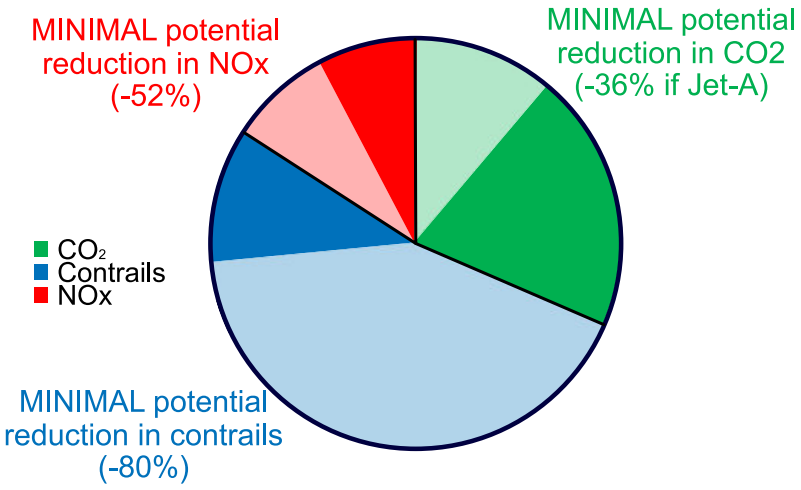

Figure 1.2: The potential reduction in radiative forcing from technology introduced within the MINIMAL project. Adapted from [2]

1.1.1 The intercooled composite cycle engine

The two key technologies that enable this extensive reduction in radiative forcing are intercooling and the composite cycle. The composite cycle combines the high power density of turbomachinery with the increased thermal efficiency of an internal combustion engine (ICE), resulting in an engine core similar to that of a high-bypass turbofan which now features constant volume combustion chambers instead of the conventional constant pressure burner. The introduction of the composite cycle engine (CCE), combined with improved aircraft performance, is the main contributor

to the reduction in fuel consumption and, consequently, CO_2 emissions. However, the CCE is expected to produce higher NOx emissions compared to a constant-pressure burner because of the increased combustion temperatures and pressures. Intercooling further enhances the performance by enabling either increased turbocharging of the air prior to combustion, reducing the overall size and weight of the engine while maintaining thermal efficiency, or reduced combustion temperatures, decreasing the NOx production. Thus, intercooling, along with exhaust gas recirculation and other technologies, provides design and operation flexibility, allowing CO_2 and NOx emissions to be balanced to minimize climate impact. Hence, intercooling is even more beneficial for the CCE than for a conventional turbofan, due to the heavy ICE and elevated combustion temperatures. Figure 1.3 illustrates an intercooled composite cycle engine and highlights the intercooler and ICE.

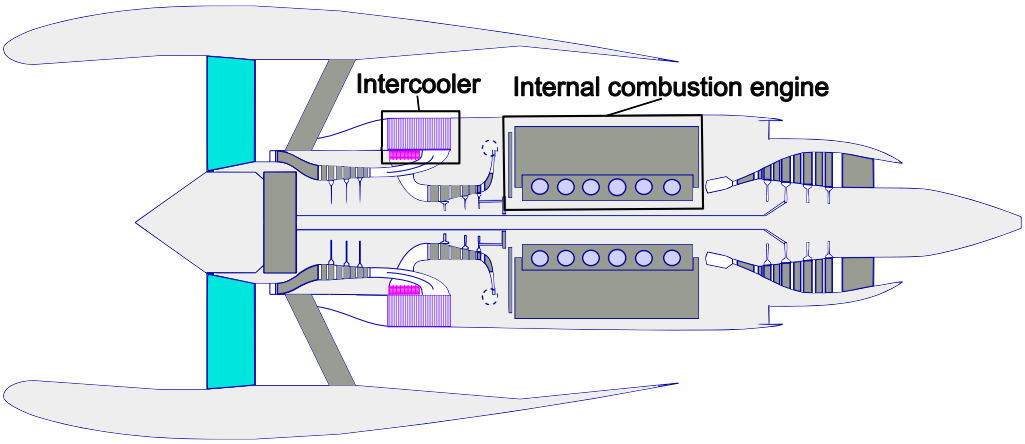

Figure 1.3: An intercooled composite cycle engine where the high pressure compressor is driven by two V12 four-stroke engines via a reduction gearbox.

1.2 Previous research on aero-engine intercooling

The Napier Nomad 1[4], illustrated in Figure 1.4, was the very first intercooled compound engine tailored for aviation and had its maiden run in 1949. It emerged as an alternative to the jet engine, offering far greater fuel efficiency due to the higher combustion pressure and temperature achievable in a reciprocating engine. The Nomad was designed to extract power from both the shaft of a diesel-powered ICE and a turbine, while utilizing a cooler situated between the axial and radial compressors to allow for a greater charge into the ICE. The Nomad 1 achieved a power output of 4,000 hp (3.0 MW) but was significantly heavier than any jet engine of comparable power. Although it was only operated a few times, it was described as an engine of "outstanding efficiency" [5]. Unfortunately, the concept was deemed too complex and heavy for further development at the time.

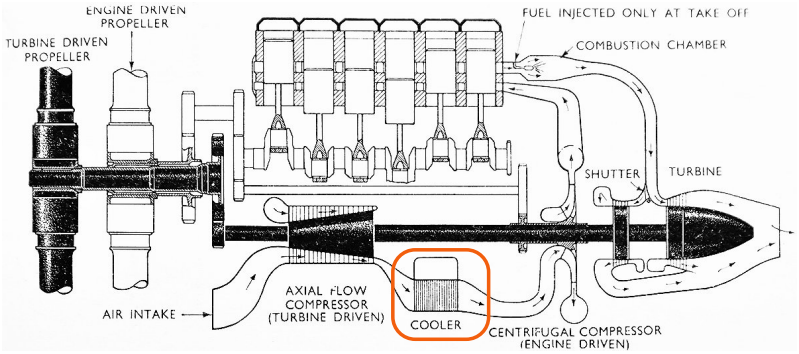

Figure 1.4: Napier Nomad 1 with highlight on its intercooler. Adapted from [6]

In 2006, the *NEW Aero engine Core concepts* (NEWAC) project [7–9] began, leading to the development of an intercooled engine core, illustrated in Figure 1.5. This design enables an overall pressure ratio higher than that of conventional engines by pushing the limits of the combustion inlet temperature. The intercooler consists of cross-corrugated plate heat exchangers, arranged in an annular zigzag configuration around the core, and uses fan discharge air as coolant. It was designed by Rolls-Royce UK and Oxford University, while adjacent ducting was designed and tested at Loughborough University [10–12].

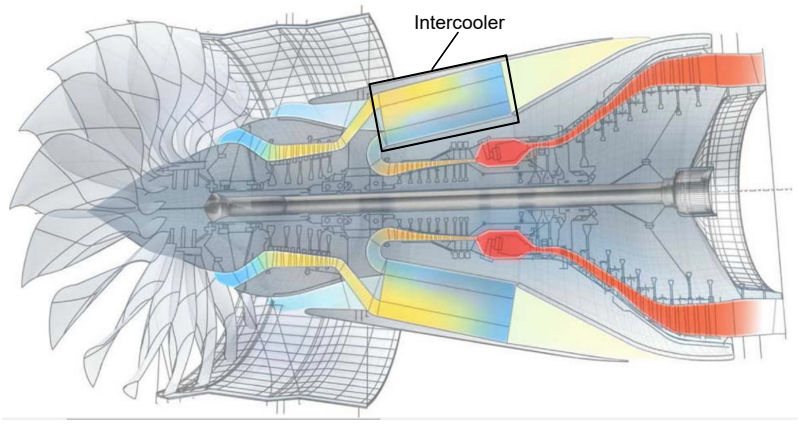

Figure 1.5: NEWAC engine with an intercooler featuring cross-corrugated plates in an annular zigzag arrangement. Adapted from [7]

Project NEWAC laid the foundation for the *Low Emissions Core-Engine Technologies* (LEMCOTEC) project [13], which began in 2011. During LEMCOTEC, an intercooled engine core, shown in Figure 1.6, was developed at Chalmers University [14–16]. The intercooler features modular segments of elliptical tubes in a two-pass, overall-counterflow arrangement, with fan discharge air as coolant. The overall-counterflow arrangement is achieved by crossing the inflow and outflow ducts, which imposes high demands on the duct design to prevent high fluid velocities and ensure sufficient diffusion prior to the heat exchanger entry. As a result, a splitter vane was included in the inflow duct.

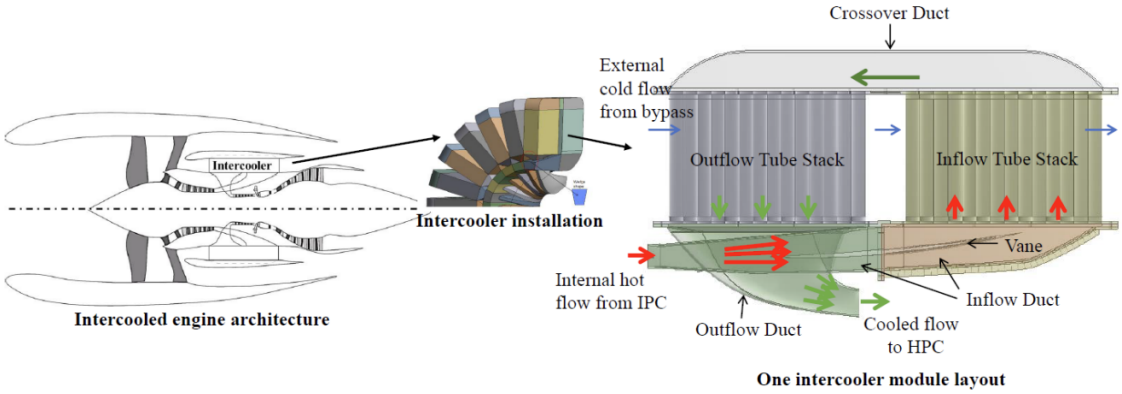

Figure 1.6: LEMCOTEC intercooled engine with an intercooler featuring elliptical tubes in a annular two-pass overall-counterflow arrangement [16]

The LEMCOTEC project was also where the first CCE was developed [17], it was not intercooled and the piston engine was used to drive a set of piston compressors. The CCE was further investigated in the *Ultra Low emission Technology Innovations for Mid-century Aircraft Turbine Engines* (ULTIMATE) project [18] which was initiated in 2015. The goal of project ULTIMATE was to compare various concepts of aircraft engines, including the first intercooled CCE, developed by Sascha Kaiser [17, 19–21]. The piston compressors were exchanged for an axial to radial turbo compressor and the introduction of the intercooler reduced the ICE weight by 20%! The intercooler was of similar design as the one used in project LEMCOTEC and used fan discharge air as coolant. Bauhaus Luftfahrt developed a similar CCE, but without the intercooler, which is illustrated in Figure 1.7. It features a core with an axial low pressure compressor, driven by a turbine, and a axial to radial high pressure compressor powered by two crankshaft-driven V10 ICEs via a gearbox.

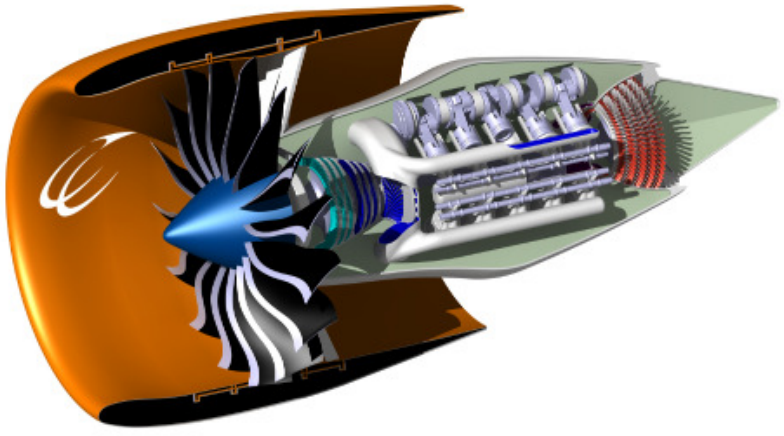

Figure 1.7: Composite cycle engine where the high pressure compressor is powered by two crankshaft-driven V10 internal combustion engines via a gearbox. It was developed by Bauhaus Luftfahrt [19, 22]

Although successful in developing some highly efficient engines, project ULTIMATE concluded that not even the introduction of radical core concepts would

be enough to achieve the environmental Flight Path 2050 targets set forth by the European Union [23, 24]. This paved the way for the investigation of alternative fuels, where one strong candidate is hydrogen. In 2018, the *ENABLing cryogEnic Hydrogen based CO2 free air transport* (ENABLEH2) project [25] was started, within which concepts were developed where hydrogen was used as coolant for the intercooler. Figure 1.8 illustrates one engine developed during ENABLEH2 which includes an hydrogen-air intercooler featuring flattened tubes with curved fins. It also includes a radial flow heat exchanger with staggered tubes which recuperate energy from a fraction of the exhaust gases to further pre-heat the fuel prior to combustion.

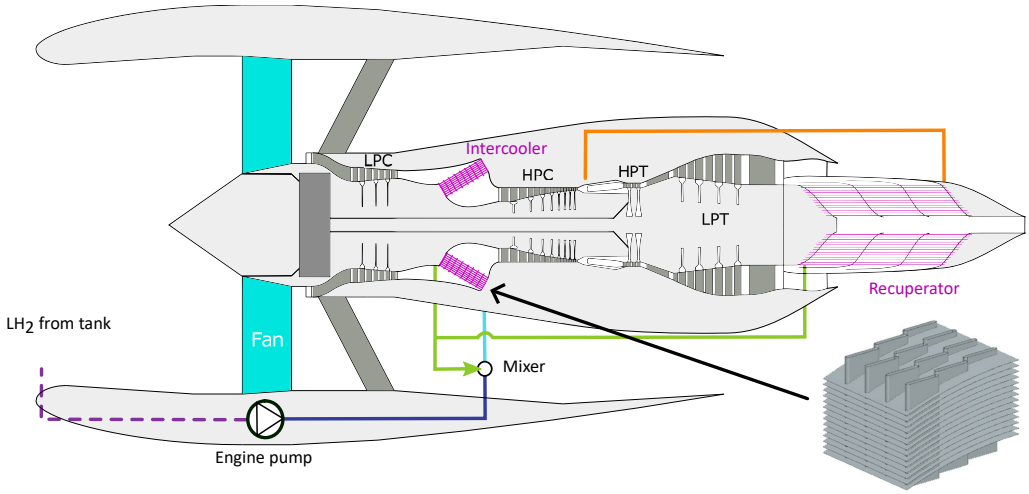

Figure 1.8: ENABLEH2 engine with both intercooler and recuperator, adapted from [26]

The projects presented above laid a solid foundation for project MINIMAL, offering significant insight into intercooling, composite cycle engines and the utilization of hydrogen. Many of the previously investigated concepts are reflected throughout this thesis, which was initialized by combining the two-pass bypass intercooler from Figure 1.6 and the fuel intercooler from Figure 1.8 into the first iteration of the hydrogen-enhanced intercooler.

1.3 Hydrogen-enhanced intercooling

The previously investigated intercooling concepts in aero engines have primarily used a fraction of the fan discharge air as coolant. However, the implementation of hydrogen as an alternative fuel could further enhance the benefits of intercooling if it is used as a coolant. Especially if stored in a cryogenic state (20 K and 2 bar), since there would be a large temperature difference between the very cold fuel (40-50 K as it reaches the engine) and the hot gas (300-700 K depending on the operating point and where in the compression process the intercooler is installed). Hydrogen has outstanding thermal properties with a specific heat capacity (c_p) which is 14-15 times higher than that of air and approximately 7 times higher than that of conventional Jet-A fuel. The high heat capacity and temperature difference mean

that a substantial amount of heat can be transferred, despite having a rather low fuel burn at a fuel-to-air ratio (FAR) of 1%. The transferred heat increases the fuel enthalpy prior to combustion and consequently lowers the fuel consumption. Transferring the same amount of heat using fan discharge air as the coolant would require a significantly heavier, and larger, heat exchanger due to the low temperature difference and large volume flow. However, initial studies on the required, and beneficial, amount of cooling for the intercooled CCE show that more heat need to be transferred than either the fuel (limited by the mass flow) or fan discharge air (limited by the low temperature difference) can receive alone. Hence, the hydrogen-enhanced intercooling concept is born, where both fan discharge air and hydrogen fuel will be used as coolants.

The utilization of cryogenic hydrogen as a coolant is not without its own challenges. One being the elevated risks of condensation and ice accretion from having a coolant at sub 0°C. Another is associated with the unstable nature of hydrogen-air mixtures, which means that leakage into the core air stream could have catastrophic consequences in the case of combustion in a compressor or during the wrong stroke of the ICE. Moreover, because of its small molecular size, hydrogen tends to diffuse into materials that can significantly degrade their structural properties, a phenomenon known as hydrogen embrittlement.

1.4 Overarching approach

Designing components for integration into a complex system such as an aircraft engine is a challenging process that often relies on collaboration. An interconnected loop of information transfer is usually formed where everyone requires input in order to make design decisions, inputs that can only be determined once the complete system is available. In the specific case of designing a heat exchanger, critical inputs are unavailable during the early stages of the project. These include the amount of heat to be transferred, the fluid conditions at the heat exchanger inlet, and trade-factors for weight, volume, and pressure loss. Consequently, it is clear that no decisions regarding heat exchanger geometry or size can be made at this stage. The loop persists because some of the required input is a recursive function of the heat exchanger itself, since; the cost of transferring heat has to be taken into account when deciding on the amount of heat to transfer. A design approach which represents the entire system using surrogate models would give more freedom and flexibility, reducing the need for assumptions and premature decisions. Once the surrogate models representing all the components are assembled, it should be possible to optimize the system as a whole and decide which components to use. One still has to decide on the bounding box, within which the surrogate model should be valid, which would preferably be as large as possible. However, extending the limits decreases the resolution and increases uncertainties. For the surrogate model representing the intercooler, the bounding box is the heat exchanger families considered, the different arrangements included, and the ducts investigated. For instance, one could never reach the decision in favor of a two-pass tubular heat exchanger with radially diffusing ducts featuring a splitter unless that configuration

was included in their study. Evidently, the limitations of the bounding box can drastically impact the final design decisions and should be chosen with great care. In this case, a "funnel down" approach is chosen where the bounding box can start very large but is gradually narrowed down as the complexity of the study increases.

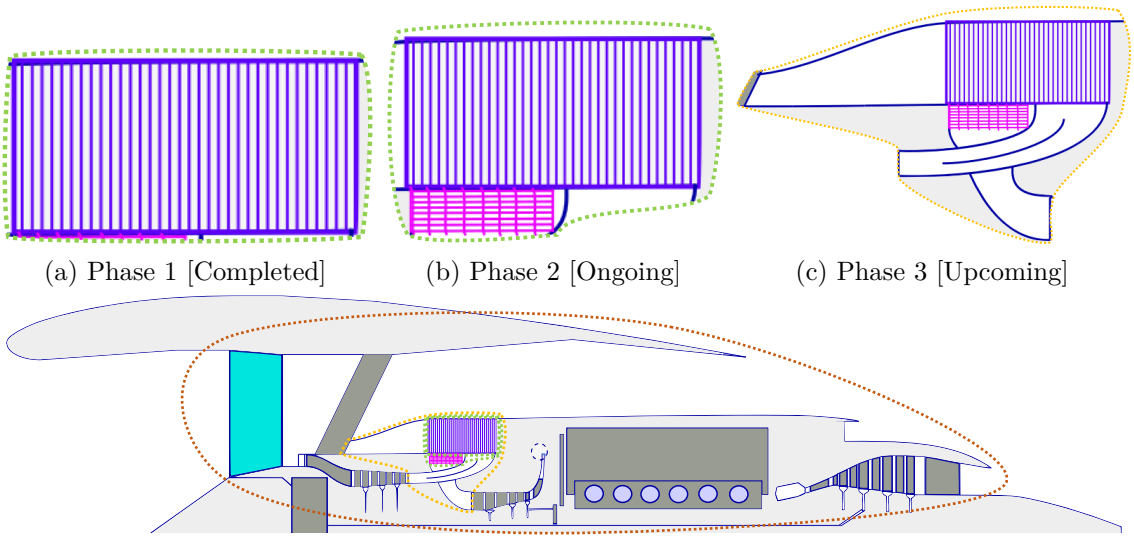

(a) Phase 1 [Completed] (b) Phase 2 [Ongoing] (c) Phase 3 [Upcoming]

(d) Phase 4 [Collaborative]

Figure 1.9: The different design phases planned for developing the hydrogen enhanced intercooler and integration into the CCE.

Four different phases can be distinguished according to Figure 1.9, where the bounding box will be narrowed down at the end of each phase based on the previous study and the parallel development of the rest of the engine. The four phases are laid out in an "Inside-Out" fashion where:

- **Phase 1 [completed]:** considers only one arbitrarily shaped heat exchanger with the aim of determining a method for estimating its aerothermal performance. Since no such method was found, this prompted the development of a novel tool (GenHEX), which is the basis for Paper 1. This tool makes it possible to estimate the aerothermal performance of a generalized heat exchanger and will be used during the upcoming phases, practically allowing the bounding box to include any possible heat exchanger configuration.

- **Phase 2 [ongoing]:** considers the coupling of a hydrogen-enhanced intercooler, where one heat exchanger transfers heat from the core-stream to the bypass-stream and the other from the core-stream to the hydrogen fuel. This study begins with a down-selection of different arrangements based on cooling potential while disregarding weight, volume, and pressure losses. The different arrangements are compared for a range of positions within the core pressurization process and a range of values for the massflow of air extracted from the bypass. Most arrangements are excluded from the bounding box for upcoming studies. One selected arrangement is studied further and the impact

of various design considerations is assessed, along with strategies to mitigate issues such as freezing and leakage. The GenHEX method is used to size the heat exchangers under different constraints in order to estimate the impact on the specific cooling power and the coefficient of performance. These studies are the basis for Paper 2.

- **Phase 3 [upcoming]:** considers the chosen arrangement from phase 2 but now includes the adjacent ducting. The objective is to evaluate the aerodynamic performance of the ducts for various lengths, area ratios, and curvature. The interaction between ducts and heat exchangers will be investigated to assess the impact on heat transfer from phenomena such as having nonuniform flow at the heat exchanger inlet and the impact on duct performance from varying the heat exchanger geometry. Validation of the duct performance will be conducted under engine representative conditions in the in-house low-pressure compressor facility.
- **Phase 4 [collaborative]:** will concern the integration of the intercooler surrogate models into the MINIMAL engine model. The engine will then be optimized for the minimum climate impact according to the findings within the project.

1.5 Outline and objectives

The present thesis is outlined as follows. In Chapter 2 Phase 1 is introduced, where a novel heat exchanger generalization method is proposed, which is further detailed in paper 1. In Chapter 3, the ongoing work during Phase 2 is presented, and the GGPs that minimize the objective function for the unconstrained case in Paper 2 are discussed. Chapter 4 gives a brief description and discussion of the methodologies used in the appended papers. The fifth and final chapter summarizes the conclusions and presents the upcoming work.

The main objective for the ongoing PhD project is to investigate the hydrogen-enhanced intercooler, which requires studies on:

- how to facilitate exploration of the heat exchanger design space
- how the hydrogen-enhanced intercooler should be arranged and where is should be positioned
- how to mitigate the risks associated with using cryogenic hydrogen as coolant
- how to effectively integrate compact heat-exchanger technology into the engine core
- what a suitable intercooler design would look like for the hydrogen-fueled intercooled composite cycle engine

and probably many more topics which will arise throughout the project.

Chapter 2

Phase 1: Generalization of a heat exchanger

Most heat exchanger design studies follow recommended design procedures, such as those provided by [27–29] and apply a case study approach when deciding which heat exchanger to use for their application. The case study approach relies on the designer to gather an initial collection of heat exchangers with known performance, which are then assessed for an application where the best solution is chosen. A simplified illustration of the case study approach is shown in Figure 2.1a, where three basic shapes represent the collection of heat exchangers that are evaluated for an aircraft application, where the circle was deemed the best solution. The case study approach is reliable and often sufficient, especially when the designer is limited to heat exchangers from a heat exchanger family, supplier or certain collection. However, it has two main limitations when it comes to less restricted design tasks. First, the final solution is inherently confined to the initial collection; the designer using the case study approach in Figure 2.1a can never get another solution than the three shapes he provided. This constraint places significant demands on the designer's intuition when selecting designs to include for the study. Second, the case study approach becomes inadequate when the application within which the heat exchanger will be used is not fully defined. For example, when designing a heat exchanger for an aircraft engine, in parallel with the development of the engine itself.

Preferably, the designer would gather a collection that is large enough to cover all possible heat exchanger configurations. However, it is more common for the designer to use intuition and assume a heat exchanger family, such as bare or finned tubes, and then gather a collection of heat exchangers of that type from a library of validated designs. One well established library of heat exchangers is provided by Kays and London [27], which is displayed in Figure 2.2. Figure 2.2a displays all heat exchangers in the library and makes it clear that limiting the collection to bare or finned tubes results in 5-20 designs which only cover a fraction of the design space. Although this is better than the simplistic example in Figure 2.1a, it still entails that not only intuition, but also luck, is required for one of these to be the globally optimum design. If the collection includes a sufficient number of discrete geometries within a heat exchanger family, interpolation along design parameters

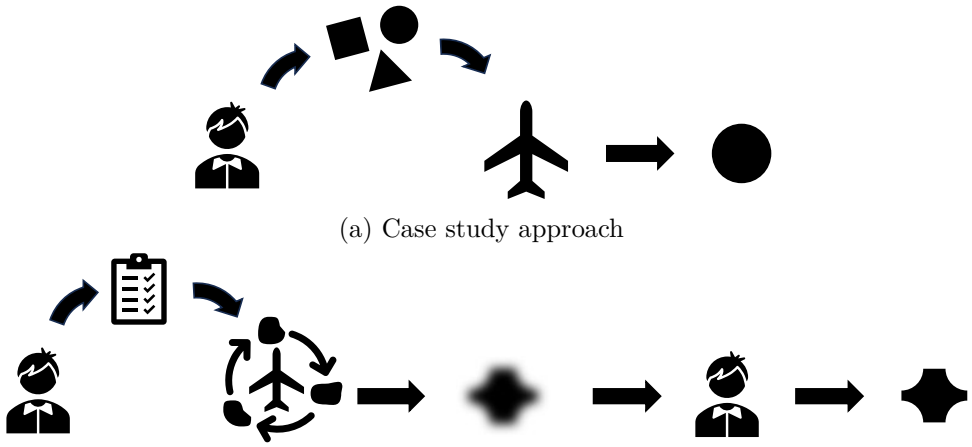

(a) Case study approach

(b) Generative approach

Figure 2.1: Artistic illustration of the commonly used case study approach versus a generative approach

can be used to estimate the performance of geometries which are not included in the collection. For example, when deciding the tube spacing of elliptical tubes or angles and amplitudes of cross corrugated plates. In this case, the design space transitions from discrete design points (as shown in Figure 2.2a) to continuous regions within the interpolated heat exchanger families (illustrated in Figure 2.2b), which greatly increase the chances of finding the optimum design, but only if it lies within the interpolated region.

To further address the limitations of the case study approach, a more versatile method was developed that facilitates a generative approach (illustrated in Figure 2.1b) in which the designer would provide design targets, and the method returns guidelines for the design of the heat exchanger. For this to be feasible, a generalized description of the heat exchanger is required, one that represents the entire design space and, thereby, completely removes the first limitation of the case study approach. This is illustrated in Figure 2.2c, where interpolation between heat exchanger families becomes possible. This generalized description supports an extensive exploration of the design space without relying on an initial collection of heat exchangers, thus reducing the need for designer intuition, luck, or access to extensive databases. Additionally, the second limitation of the case study approach was countered by aiming at developing a lightweight method that relies on a reduced number of parameters, which can be implemented as a surrogate model for full system evaluations. This enables the use of application-tailored heat exchangers even during early-stage design without significantly increasing computational complexity.

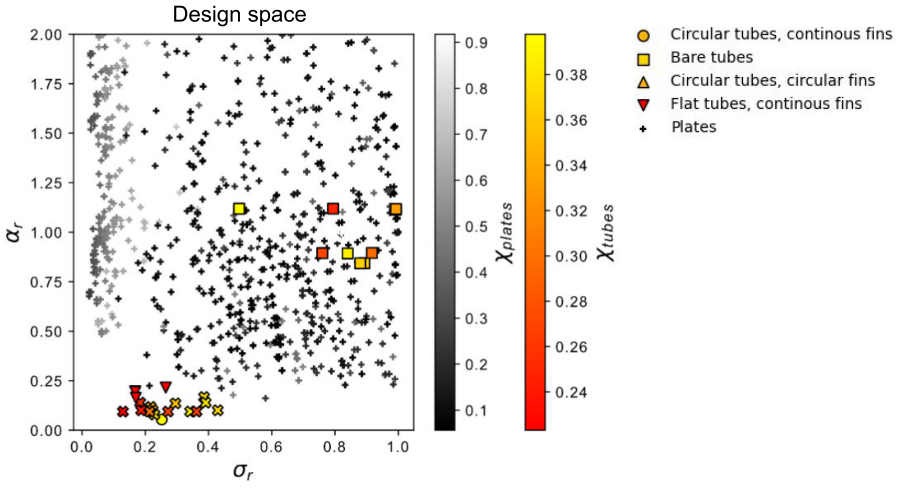

(a) Discrete

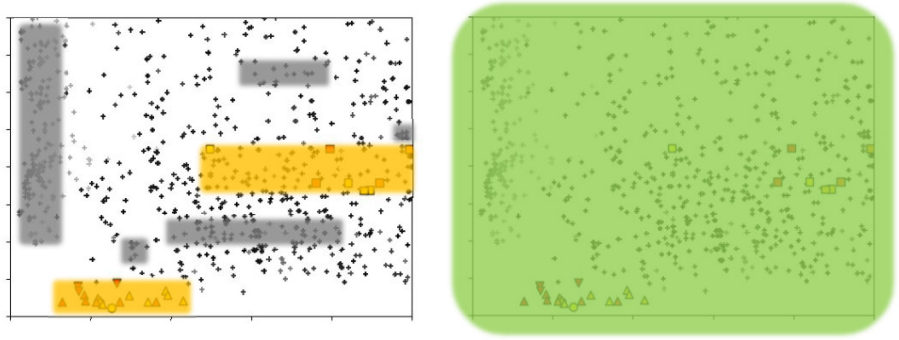

(b) Interpolated

(c) Generalized

Figure 2.2: Design space based on the experimentally validated collection of heat exchangers presented by Kays and London [27]. The axes and colorbar are the geometrical generalization parameters σ_r, α_r and χ described in section 2.1.

2.1 The generalized heat exhanger (GenHEX) design and evaluation method

The first goal in obtaining the generalized heat exchanger description is to establish design parameters that can be maintained regardless of the heat exchanger family. The second goal is to reduce the number of design parameters, while fully defining the heat exchanger geometry, in order to facilitate easy design space exploration. The result is a set of geometrical generalization parameters (GGPs), where any given heat exchanger can be described by one unique set of GGPs. The reverse is not true; there can be a near-infinite number of different heat exchangers for a given set of GGPs. Hence, the designer is still required to decide which heat exchanger to use in the end, but the generative approach provides recommendations for the heat exchanger's design features, such as free-flow and surface areas. The geometrical generalization of the heat exchanger is valid for any rectangular cuboid heat exchanger with fluids flowing from one side to the opposite with a constant flow area. There are some cases in which this would not hold true; tubular designs

with unstaggered tubes are one example, but most of these have poor performance because they are prone to flow instabilities and separation, resulting in high pressure losses. In the next section (Section 2.1.1), I provide a complete explanation of the generalized geometrical formulation, leading to the derivation of the geometrical generalization parameters σ_r, α_r, and χ, which span the design space in Figure 2.2. In Section 2.1.2 I will discuss the different methods that were considered to estimate the aerothermal performance for this generalized geometry.

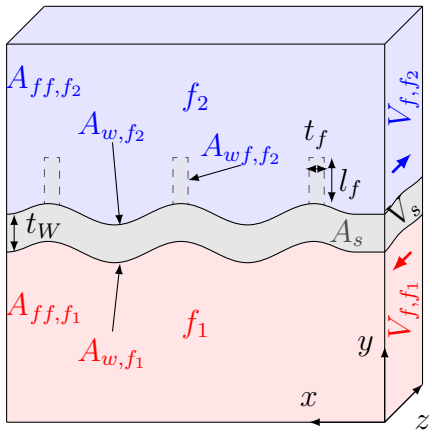

- Frontal area : $A_{fr} = \underline{L_x L_y}$
- Free-flow area : $\underline{A_{ff}}$
- Solid cross section area : $\underline{A_s}$
- Wetted surface area : $\underline{A_w}$
- Wetted fin surface area : $\underline{A_{wf}}$
- Total volume : $V_t = \underline{L_x L_y L_z}$
- Solid volume : V_s
- Fluid volume : V_f
- Wall thickness : $\underline{t_W}$
- Fin thickness : $\underline{t_f}$
- Fin length : $\underline{l_f}$

Figure 2.3: General representation of a counterflow heat exchanger transferring heat between two fluids (f_1, f_2).

2.1.1 Geometrical formulation

Figure 2.3 illustrates a heat exchanger in a counterflow configuration containing two fluids (f_1, f_2) separated by a solid structure. However, not that the derivations below are independent of whether the heat exchanger is a counterflow, crossflow, or parallel flow configuration.

At this stage, 12 inputs are required and there is a high risk of over-defining the heat exchanger; for example if providing free-flow areas which together are greater than the frontal area. The risk of over-defining the geometry can be resolved and the amount of inputs required can be reduced by including some purely geometrical equations. First, the total volume (V_t) can be assembled by the fluid (V_f) and solid (V_s) volumes as:

$$V_t = V_{f,f_1} + V_{f,f_2} + V_s \tag{2.1}$$

Then, under the assumption of constant free flow areas for both f_1 and f_2 along their respective flow axis (L), Eq 2.1 can be rewritten as:

$$V_t = A_{ff,f_1} L + A_{ff,f_2} L + V_s \tag{2.2}$$

$$\Rightarrow 1 = \frac{A_{ff,f_1} L}{V_t} + \frac{A_{ff,f_2} L}{V_t} + \frac{V_s}{V_t} \tag{2.3}$$

Further, expressing the total volume and frontal areas using the outer dimensions, Eq 2.1 can be rewritten as:

$$1 = \frac{A_{ff,f_1} L}{L_x L_y L_z} + \frac{A_{ff,f_2} L}{L_x L_y L_z} + \frac{V_s}{V_t} \tag{2.4}$$

$$= \frac{A_{ff,f_1}}{A_{fr,f_1}} + \frac{A_{ff,f_2}}{A_{fr,f_2}} + \frac{V_s}{V_t} \tag{2.5}$$

Finally, by introducing the void fraction ($\sigma = A_{ff}/A_{fr}$) and the solid volume fraction ($\chi = V_s/V_t = A_s/A_{fr}$), which is also known as compactness or the opposite of the porosity defined by Kays and London [27], Eq 2.5 can be rewritten into the generalized volume expression:

$$1 = \sigma_{f_1} + \sigma_{f_2} + \chi \tag{2.6}$$

Using a similar approach, the solid volume can be expressed by:

$$V_s = (A_{w,f_2} + A_{w,f_1}) \frac{t}{2} \tag{2.7}$$

where A_w is the wetted surface areas and t is an average structural thickness (presented below). Equation 2.7 can be rewritten by dividing both sides in Eq 2.7 by V_t and introducing the surface area density ($\alpha = A_w/V_t$), as:

$$\chi = (\alpha_{f_1} + \alpha_{f_2}) \frac{t}{2} \tag{2.8}$$

where Eq. 2.8 is the generalized surface expression. The average structural thickness can be expressed as a surface-weighted average of the finned surfaces (A_{wf}), with thickness t_f, and un-finned surfaces (A_w), with thickness t_W, as:

$$t = \frac{t_W(A_{w,f_1} - A_{wf,f_1}) + t_W(A_{w,f_2} - A_{wf,f_2}) + t_f A_{wf,f_1} + t_f A_{wf,f_2}}{A_{w,f_1} + A_{w,f_2}} \tag{2.9}$$

In the specific case of equal fin and wall thickness, it follows that $t = t_W = t_f$.

Designs with fins protruding into both fluids would have reduced overall surface efficiency compared to designs which instead achieve more surface area by increasing the number of tubes, plates, or channels. However, if the fins are intended to enhance fluid mixing or direct the flow, having them on both sides could be a deliberate and effective design choice. For the sake of simplicity, it is assumed that fins are only present on the f_2 side, as illustrated in Figure 2.3, and that the area where the fin connects to the wall is much smaller than the total surface area, such that $A_{wf,f_2} = A_{w,f_2} - A_{w,f_1}$. With these assumptions, the averaged structural thickness

can be simplified as follows:

$$t = \frac{t_W A_{w,f_1} + t_W \left(A_{w,f_2} - A_{wf,f_2}\right) + t_f A_{wf,f_2}}{A_{w,f_1} + A_{w,f_2}} \tag{2.10}$$

$$= \frac{2t_W A_{w,f_1} + t_f \left(A_{w,f_2} - A_{w,f_1}\right)}{A_{w,f_1} + A_{w,f_2}} \tag{2.11}$$

$$= \frac{2t_W \alpha_{f_1} + t_f \left(\alpha_{f_2} - \alpha_{f_1}\right)}{\alpha_{f_1} + \alpha_{f_2}} \tag{2.12}$$

$$= t_W \frac{2\alpha_{f_1}}{\alpha_{f_1} + \alpha_{f_2}} + t_f \frac{\alpha_{f_2} - \alpha_{f_1}}{\alpha_{f_1} + \alpha_{f_2}} \tag{2.13}$$

$$= t_W \frac{2\alpha_{f_1}}{\alpha_{f_1} + \alpha_{f_2}} + t_f \sigma_{ftt} \tag{2.14}$$

Where σ_{ftt} is the finned-to-total surface area, derived as:

$$\sigma_{ftt} = \frac{A_{wf,f_2}}{A_{w,f_1} + A_{w,f_2}} \tag{2.15}$$

$$= \frac{A_{w,f_2} - A_{w,f_1}}{A_{w,f_1} + A_{w,f_2}} \tag{2.16}$$

$$= \frac{\alpha_{f_2} - \alpha_{f_1}}{\alpha_{f_1} + \alpha_{f_2}} \tag{2.17}$$

The void fraction ratio ($\sigma_r = \sigma_{f_1}/\sigma_{f_2}$) and surface area density ratio ($\alpha_r = \alpha_{f_1}/\alpha_{f_2}$) are introduced, that together with χ are denoted as the geometrical generalization parameters (GGPs). Equations 2.6 and 2.8 can then be rewritten as:

$$(2.6) \rightarrow \sigma_{f_2} = \frac{1 - \chi}{\sigma_r + 1} \tag{2.18}$$

$$(2.8) \rightarrow \alpha_{f_2} = \frac{2\chi}{t\left(\alpha_r + 1\right)} \tag{2.19}$$

The introduction of the GGPs and the derivation of Eqs 2.18 and 2.19 result in a reduction of the number of required inputs from twelve down to eight, which are sorted into three categories:

Outer dimensions:
- L_x
- L_y
- L_z

Structural:
- t_W
- t_f

GGPs:
- σ_r
- α_r
- χ

Together with Eqs 2.14, 2.17, 2.18 and 2.19, these parameters fully define the geometry of the heat exchanger and allow for the calculation of the free-flow areas, surface areas, finned-surface area and solid volume. It can also be proven that these equations hold true for configurations other than counter-flow; the only difference is that A_{fr} will vary for each fluid. Illustrations showing how the geometry changes by varying the GGPs are provided in Figure 2.5.

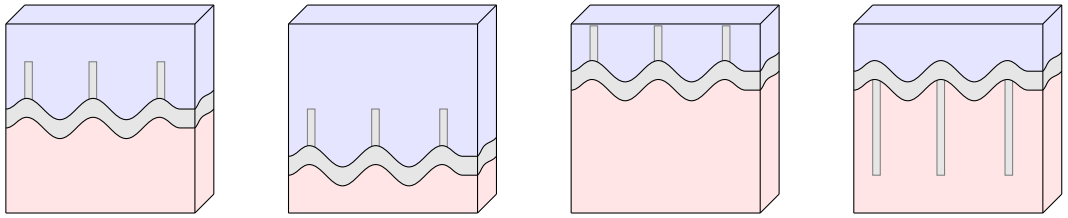

(a) $\sigma_r \approx 1$, $\alpha_r < 1$ (b) $\sigma_r < 1$, $\alpha_r < 1$ (c) $\sigma_r > 1$, $\alpha_r < 1$ (d) $\sigma_r > 1$, $\alpha_r > 1$, χ increased

Figure 2.5: General representation of a heat exchanger illustrating how the geometry change for a few combinations of the geometrical generalization parameters.

2.1.2 Estimating the aerothermal performance

Estimating the aerothermal performance of a generalized geometry is a challenging task, particularly when the geometry is not unique for a given set of GGPs. The goal is, therefore, to estimate the "state-of-the-art" performance achievable by the best design for a given set of GGPs, resulting in correlations that facilitate exploration of the design space. Ultimately, the designer must identify a high-performance design featuring the recommended GGPs to achieve the estimated performance. First, the hydraulic diameter (D_h) and Reynolds number (Re) for each passage and fluid can be defined as:

$$D_h = 4\frac{\sigma}{\alpha} \tag{2.20}$$

$$\mathrm{Re} = \frac{\dot{m} D_h}{\sigma A_{fr} \mu} = \frac{4\dot{m}}{\alpha A_{fr} \mu} \tag{2.21}$$

Then, the definition of the overall heat transfer coefficient (U) for the f_1 side can be rewritten (with α) as:

$$\frac{1}{U_{f_1}} = \frac{1}{(\eta_o h)_{f_1}} + \frac{\alpha_r}{(\eta_o h)_{f_2}} + \frac{2t}{\left(1 + \frac{1}{\alpha_r}\right) k} \tag{2.22}$$

where η_o is the overall surface efficiency and h is the heat transfer coefficient for convection. The overall surface efficiency is 1 (100%) on the side of the heat exchanger without fins but is otherwise a function of the fin efficiency (η_f), expressed as:

$$\eta_{o,f_2} = 1 - \sigma_{ftt,f_2}\eta_f \tag{2.23}$$

$$\sigma_{ftt,f_2} = \frac{\alpha_{f_2} - \alpha_{f_1}}{\alpha_{f_2}} \tag{2.24}$$

$$\eta_f = \frac{\tanh(ml_f)}{ml_f} \tag{2.25}$$

$$ml_f = \frac{l_f}{\sqrt{t_f}} \sqrt{\frac{2h_{f_2}}{k_f}} \tag{2.26}$$

where k_f is the thermal conductivity of the fin material. The fin characteristic dimension ($l_f/\sqrt{t_f}$) must be provided to calculate the overall surface efficiency. This characteristic dimension is similar to an aspect ratio but is not dimensionless.

The pressure loss for each fluid through the matrix, excluding entry and exit losses, is calculated as:

$$\Delta p_0 = \frac{\dot{m}^2}{2\rho_{in}A_{fr}^2}\left(\left(\frac{1}{\sigma^2}+1\right)\left(\frac{\rho_{in}}{\rho_{out}}-1\right)+2fL\frac{\alpha}{\sigma^3}\frac{\rho_{in}}{\rho_m}\right) \tag{2.27}$$

where ρ is the fluid density which should be provided at both the inlet and outlet, along with a representative mean value. For most fluids, the mean value can be approximated using the midpoint density, as their density typically varies linearly with temperature. However, for fluids with non-linear properties, such as cryogenic hydrogen, a more representative mean value is obtained through integration. In Eq. 2.27, L represents the length of the heat exchanger in the flow direction, and f denotes the Fanning friction factor [29]. A cautionary note: both the Darcy friction factor [29] and the Fanning friction factor are sometimes denoted f, but the Darcy friction factor is defined as four times the Fanning friction factor!

Aerothermal coefficients

Now, to address the problem at hand: how do we estimate the "state-of-the-art" heat transfer and pressure loss for a generalized geometry? Luckily, the only remaining unknowns are the heat transfer and friction coefficients. Where h is often expressed in terms of the Nusselt number (Nu) or the Colburn factor (j), which are dimensionless and more general, making them scalable for different sizes and fluids. One approach for estimating these coefficients is to use the modified Reynolds or Chilton–Colburn analogy, which relates the transport of momentum to the transport of heat. This essentially states that no heat transfer can occur without associated friction, such that:

$$\frac{f}{2} = \frac{h}{c_p u \rho \mathrm{Pr}^{1/3}} = \frac{\mathrm{Nu}}{\mathrm{RePr}^{1/3}} = j \tag{2.28}$$

where c_p is the specific heat capacity at constant pressure, u is the fluid velocity, and Pr is the Prandtl number, which is defined as the ratio of momentum diffusivity to thermal diffusivity. There is still a need to estimate either the heat transfer or the friction, but using the relationship in Eq 2.28 to calculate the other can provide results resembling the theoretical optimum for heat transfer. Although the analogy is correct in the fact that no heat transfer can occur without friction, the reverse is not true. Most heat exchangers experience additional pressure loss due to small-scale turbulence. In simple terms, higher velocity near the walls lead to more friction, but also a larger temperature gradient which enhances heat transfer (as illustrated in Figure 2.6). However, small-scale turbulence, caused by flow separations or rapid velocity changes, heats the fluid itself and leads to the loss of useful energy. An attempt can be made to estimate the deviation of "state-of-the-art" heat exchangers from the Reynolds analogy and use this to estimate aerothermal performance. However, this approach was not chosen for the current work.

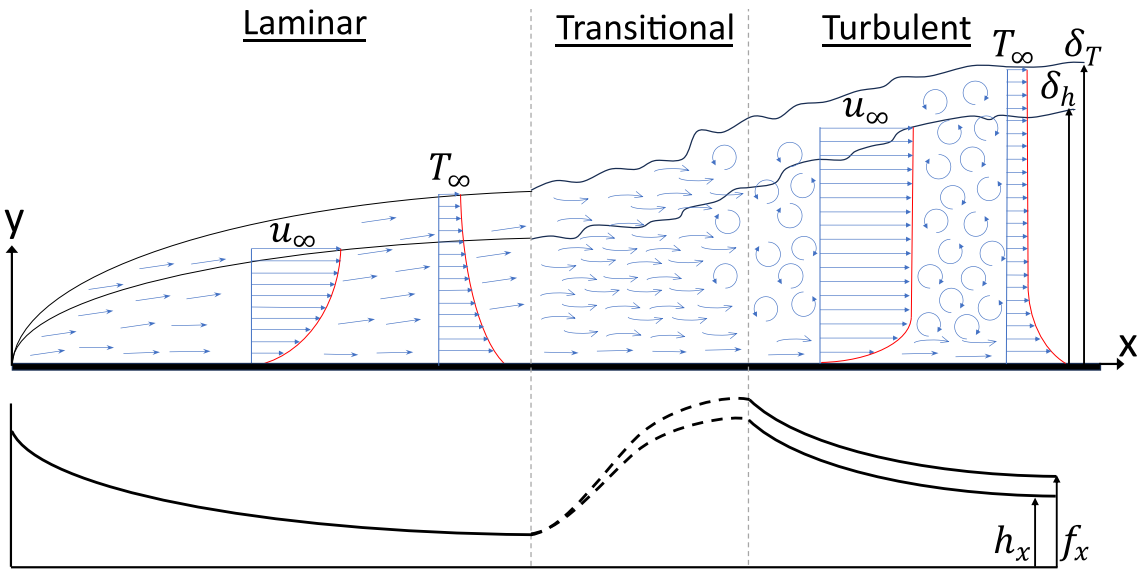

Figure 2.6: Boundary layer development for the momentum and thermal boundary layers of thickness (δ) with displayed velocity (u) or temperature (T) gradients. Also the resulting trend in local heat transfer (h_x) and friction coefficients (f_x). Note that no axises are to scale and that the figure is purely illustrational!

Another method of estimating heat transfer and friction is to approximate that all surfaces behave like a flat plate and integrate the boundary layers of momentum and temperature, as illustrated in Figure 2.6. An approach could be to allow for shorter structures such that the boundary layer is disrupted and restarted with no boundary layer thickness. This is a common heat transfer enhancement method, as heat transfer is higher at low boundary layer thickness because the fluid is at the free-stream temperature near the wall. However, the fluid also has a freestream velocity, resulting in high friction. The laminar Prandtl number (Pr) is a fluid property that remains constant during the development of the laminar boundary layer. This implies that the ratio of local heat transfer to friction coefficient is also constant, in accordance with the Reynolds analogy. As the flow transitions to a turbulent boundary layer, the turbulent Prandtl ($\mathrm{Pr_t}$) number should be used. Although the turbulent Prandtl number is not as easily defined, it is lower than the laminar one, and thereby the heat transfer to friction ratio will be lower for a turbulent boundary layer, even though the absolute values of local heat transfer and friction are higher, illustrated in Figure 2.6. Accurately estimating when the boundary layer would transition from laminar to turbulent is already quite challenging for a flat plate parallel to the freestream. And it becomes even more complicated when trying to account for common heat transfer enhancement methods such as angling the plates relative to the freestream or when trying to expand the method to account for curved surfaces. Hence, neither this approach was chosen.

Fortunately, others have also tried to derive a more generalized method to estimate the aerothermal performance of heat exchangers. LaHaye et al. [30] managed to related the aerothermal performance of the heat exchangers presented by Kays and London [27] as a function of the Reynolds number and a ratio of the undisturbed flow length to hydraulic diameter (ℓ/D_h). They defined the undisturbed flow length

for different types of heat exchangers, as shown in Figure 2.7a, and successfully demonstrated a clear trend, which is recreated in Figure 2.7b. The outlier at $\ell/D_h = 0.95$ corresponds to a heat exchanger featuring un-staggered tubes, which has been previously mentioned as an example of a poor design.

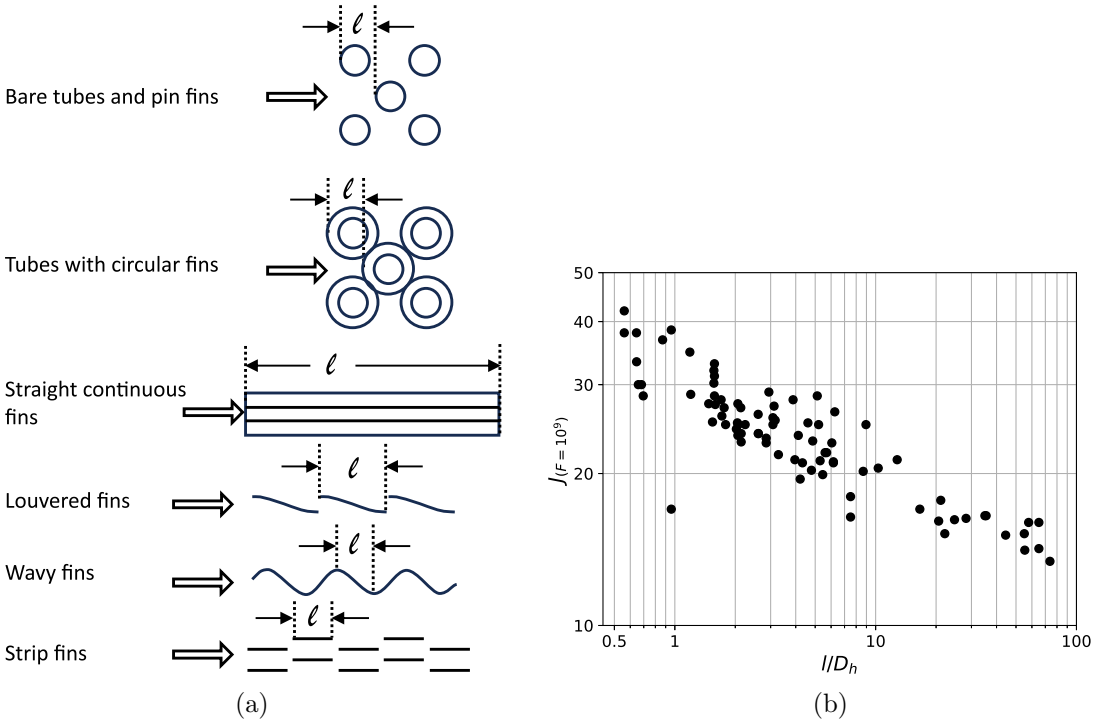

(a) (b)

Figure 2.7: a) Adapted illustration of the undisturbed flow length (ℓ) as defined for various HX types by LaHaye et al.[30]
b) Heat transfer performance factor ($J = jRe$) versus undisturbed flow length divided by the hydraulic diameter (ℓ/D_h) for multiple heat exchangers. The conditions vary such that all heat exchangers operate at a pumping power factor ($F = fRe^3$) of $F = 10^9$.

In Paper 1 we decided to follow a similar approach to LaHaye et al. and use a regression analysis to establish expressions for the Colburn factor and the friction coefficient based on Re and the fraction $\ell/D_h = \ell\alpha/4\sigma$. The initial expressions used for the regression included a large number of terms with varying dependences for Re and ℓ/D_h. The terms of low impact were removed in order to simplify the expression, after which new coefficients were calculated. Ideally, heat exchangers of poor design or operating off their design point would be discarded or weighted less when calculating the coefficients. However, due to lack of an accurate metric for correctly deciding how the different heat exchangers should be weighted, all heat exchangers shown in Figure 2.2 were included and weighted equally, which eventually

led to the correlations presented in paper 1:

$$j = 0.360 \left(\frac{\ell}{D_h} \right)^{-0.401} \mathrm{Re}^{-0.413} + 2.13 \times 10^{-05} \left(\frac{\ell}{D_h} \right) \tag{2.29}$$

$$f = 0.492 \left(\frac{\ell}{D_h} \right)^{-0.501} \mathrm{Re}^{-0.232} \tag{2.30}$$

> *"In the range of* $0.645 < \ell/D_h < 73.8$ *and* $2000 < Re < 20000$ *the correlations have an accuracy on* j *of* $\pm 25\%$ *for 94% of the data points and* f *of* $\pm 25\%$ *for 69% of the data points. For* j *all experimental points are within an error of* $\pm 40\%$*, for* f *all points are within an error of* $\pm 60\%$*."*

It should be further emphasized that the goal is not to match the performance of all heat exchangers but rather to match that of "well-designed" ones. Therefore, calling the deviation in j or f an error is misleading. In addition, designs with high values for heat transfer will most likely also have high values for friction, leading one to think of grading the heat exchanger designs based on the heat transfer to friction ratio. However, a high value on that ratio is often associated with large volumes and high weights, resulting in the need of an objective function specific to the application within which the heat exchanger is to be used to accurately grade the heat exchangers. A procedure to define such an application specific objective function was provided in Paper 1 and Paper 2.

2.2 Main contributions

The main contribution of completing Phase 1 is the novel method that enables low cost and rapid exploration of the design space, reducing the dependency on intuition in the early design stages and reducing the risk of limiting end-performance by making premature decisions. Under fixed outer dimensions, material, structure thickness, undisturbed flow length, and fin characteristic dimension, the design depends on only three parameters: the geometrical generalization parameters σ_r, α_r, and χ. These parameters govern how much solid volume should be in the heat exchanger and how the surface and free-flow areas should be distributed between the two streams. Three parameters may be few enough to enable implementation of the method into larger system models. Figure 2.8 illustrates the design steps taken when applying the method to an example case. The first step, shown in Figure 2.8a, is to explore the design space using the generalized method. Step two, depicted in Figure 2.8b, is to extract all solutions that yield the targeted heat transfer. These solutions should be graded according to an application-specific objective function to determine which performs best. Step three, shown in Figure 2.8c, is to translate the generalized geometry into an actual design. This can usually be done in multiple ways; here, I choose to design a cross-corrugated plate heat exchanger since the previous stages indicate that the surface areas on both sides should be equal. Step four, illustrated in Figure 2.8d, is not strictly required, but I chose to compare our

results to an existing design with experimentally validated results. It is worth noting that the estimated performance lies between two designs of cross-corrugated plate heat exchangers with differing corrugation angles. Since this design detail is too complex to replicate in the correlations used for estimating the Colburn and friction factors, I conclude that my method provides reasonable results that are comparable to state-of-the-art designs.

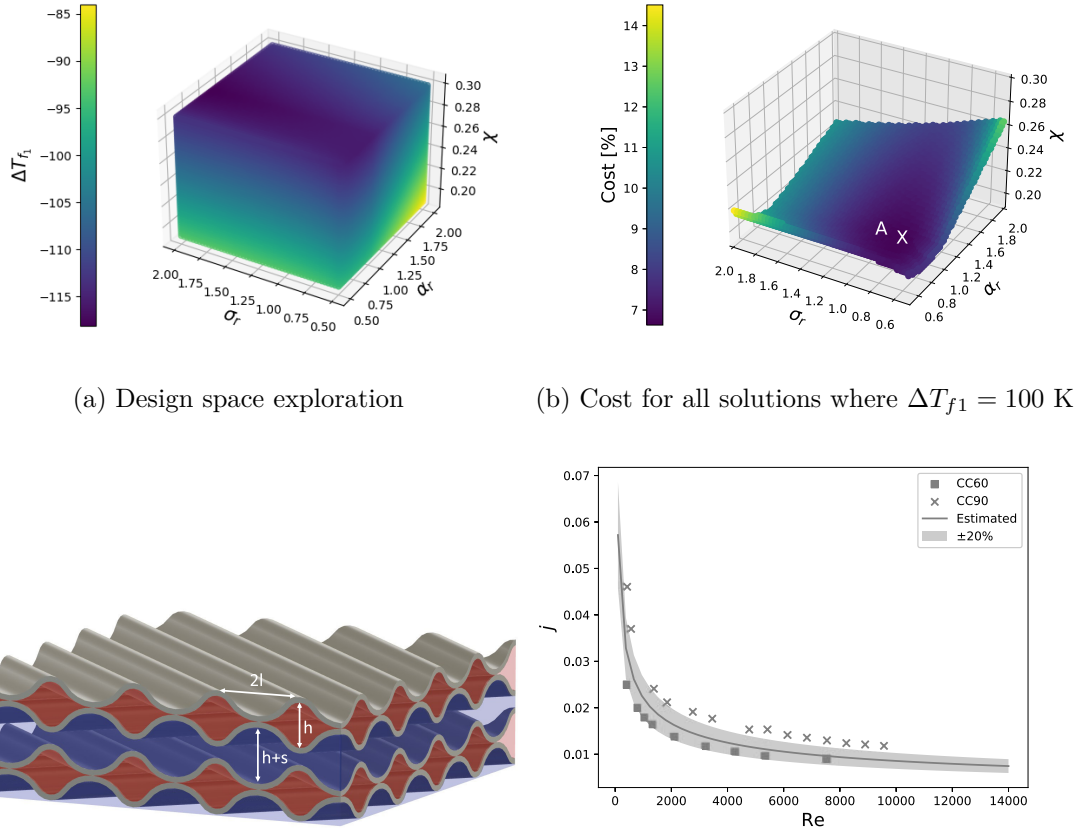

(a) Design space exploration

(b) Cost for all solutions where $\Delta T_{f1} = 100$ K

(c) One design matching the best solution

(d) Validation of performance

Figure 2.8: GenHEX design framework extracted from Paper 1

Chapter 3

Phase 2: Arranging the hydrogen-enhanced intercooler

The MINIMAL engine will be fueled by hydrogen, stored at a very low temperature. This creates a synergistic opportunity, as the core stream benefits from being cooled while the fuel needs to be heated. A core-air to hydrogen heat exchanger will be smaller and more compact than a core-air to bypass-air heat exchanger transferring the same amount of heat. However, it is likely that the required cooling for the composite cycle engine will exceed the capacity of the core-air to hydrogen heat exchanger alone, as the coolant flow (in this case, the fuel flow) is limited and ideally minimized. Therefore, coupling a core-air to bypass-air heat exchanger with a core-air to hydrogen heat exchanger in a hydrogen-enhanced intercooler configuration could offer significant benefits. This coupling can be implemented in various configurations, as illustrated in Figure 3.1, where the cooling potential for each arrangement is displayed in the case of heat exchangers at 100% effectiveness (middle row) and when the air-air heat exchanger operates at 70% and the hydrogen-air heat exchanger operates at 95% (bottom row). The cooling potentials are displayed for various values of the pressure ratio split exponent, which determines how much pressurization occurs in the core stream before and after the intercooler, and the coolant flow ratio, which governs the amount of mass flow extracted from the bypass to use as coolant.

The absence of a complete system model further complicates the situation, preventing a holistic view of the entire engine from being achieved. Hence, conclusions about the optimal value of the pressure ratio split exponent or the coolant flow ratio cannot be drawn. However, conclusions from the comparison of the arrangements illustrated in Figure 3.1 can still help limit the scope of the intercooler design before moving on to the use of more detailed analysis methods. The first part of Phase 2 relies on semi-idealized heat exchangers and compares the cooling potential of the different arrangements while disregarding the impact from weight, volume, and pressure losses. Whereas the latter parts of Phase 2 incorporate the GenHEX method in order to estimate the variations in weight and pressure losses depending on the pressure ratio split exponent and coolant flow ratio. The resulting variations in specific cooling power and coefficient of performance, illustrated in Figure 3.2, can help to derive a surrogate model that can be used for engine evaluation. Additional

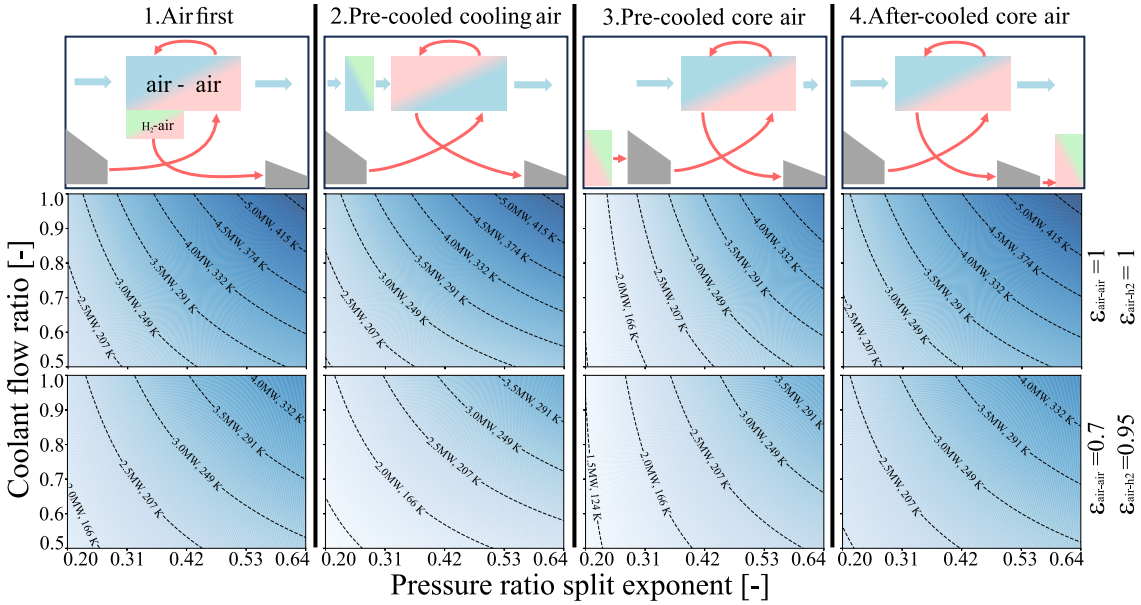

Figure 3.1: Various arrangements possible for hydrogen-enhanced intercooling.

design aspects such as the risk of ice accretion, how to minimize the risk of hydrogen leaking into the core-air stream, and how the choice of material and structure thicknesses impact the design are discussed, and the GenHEX method is used to calculate their respective impacts on the intercooler performance.

3.1 Additional discussion of results from Paper 2

The GenHEX method developed during Phase 1 is used to size the heat exchangers during the final parts of Paper 2. The optimal combination of GGPs for each value of the pressure ratio split exponent and the coolant flow ratio is determined by minimizing an objective function that calculates the impact on fuel burn from variations in weight and pressure losses.

Figure 3.2 displays the specific cooling power and the coefficient of performance for an unconstrained version of a hydrogen-enhanced intercooler in air-first arrangement, developed in Paper 2. It is unconstrained in the sense that it does not include any further mitigation methods to reduce the risk of freezing, leakage, or structural failure. Both the specific cooling power and the coefficient of performance increase towards the lower right corner, the highest value of the pressure ratio split exponent and the lowest value of coolant flow ratio. The heat transfer increases as the core air stream is further pressured and thereby heated, but decreases when the amount of bypass-air (coolant) is reduced. Moreover, the combined fluid volume in the heat exchanger is decreased as the core air is further pressurized and less air is extracted from the bypass, both contributing to a reduction in fluid velocities and thereby pressure losses.

The above mentioned impacts from varying the pressure ratio split exponent and the coolant flow ratio are reflected in Figure 3.3, which shows the GGPs for the

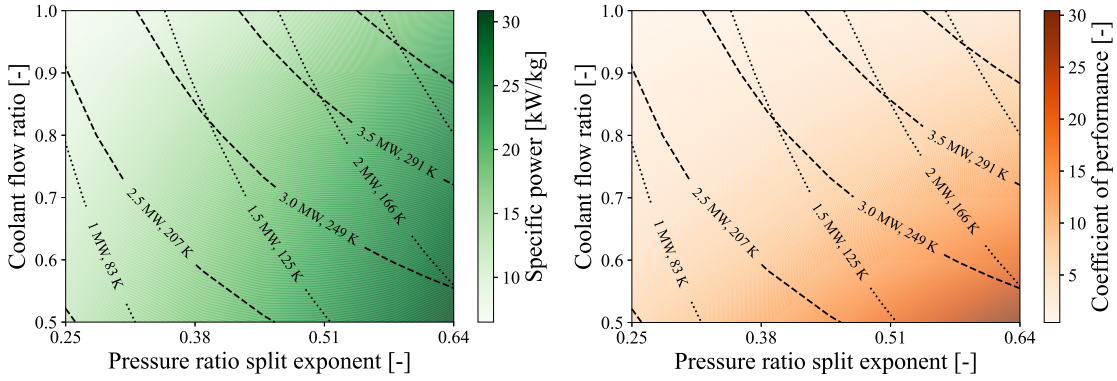

(a) Specific cooling power

(b) Coefficient of performance

Figure 3.2: Colorbar showing either the specific cooling power or the coefficient of performance for an unconstrained intercooler of the air-first arrangement, dotted lines represent the local cooling over the intercooler (Q_c and ΔT_c) while dashed lines represent the equivalent cooling at PE inlet (Q_3 and ΔT_3)

designs in Figure 3.2. In the air-air heat exchanger the core-air is denoted as f_1 and the bypass-air is denoted f_2 when defining the GGPs according to Section 2.1.1. In the hydrogen-air heat exchanger the hydrogen is denoted as f_1 and the core-air is denoted as f_2, this might seem confusing but the main reason is that this allows most of the GGPs to be varied in the range between 0-1, facilitating the optimization setup.

- **Figure 3.3a** shows the void fraction ratio in the air-air heat exchanger and that there is a strong coupling to the relative volume flow. A high value of free-flow area is provided for the core stream for low values of core-air pressurization and low amount of air extracted from the bypass (lower left corner). Whereas a high value of free-flow area in the bypass-stream is required when the core-air stream is pressurized and there is an equal mass flow in the core-air stream and the bypass-air stream (upper right corner)

- **Figure 3.3b** shows the surface area density ratio in the air-air heat exchanger and that equal surface area should be used for both streams when the mass flow is equal (upper region), whereas one should incorporate fins in the bypass when the amount of air extracted from the bypass is reduced (lower region). This is likely due to the lower cost of pressure losses occurring in the bypass-air stream compared to the core-air stream, and the decrease in heat capacity rate in the bypass-air stream resulting in a C_{min}/C_{max} further below 1.

- **Figure 3.3c** shows the solid volume fraction in the air-air heat exchanger. The solid structure (surface area) required to reach an effectiveness of 70% is the highest when the core-air stream is barely heated but there is a lot of coolant (top left corner). Since the bypass-air stream features the lower value of heat capacity rate (C_{min}) it governs the total amount of heat to be transferred for a given effectiveness. So (in the top left corner) there is a lot of heat to be transferred with a very low temperature difference, hence large surface areas are required.

- **Figure 3.3d** shows the void fraction ratio in the hydrogen-air heat exchanger, which is modeled in counter-flow arrangement. The free-flow area required by the fuel is very low compared to that of the air-stream, and the lowest value is reached when the core stream is at low pressure, hence high volume flow.

- **Figure 3.3e** shows the surface area density ratio in the hydrogen-air heat exchanger. It shows that there should be a substantial amount of fins on the core-air side of the heat exchanger. The ratio of surface area in the hydrogen stream to core-air stream is rather constant and the small, sporadic, fluctuations are an artifact of the optimization routine, presented in Section 4.2.1.

- **Figure 3.3f** shows the solid volume fraction in the hydrogen-air heat exchanger. Since the hydrogen has a lower value of the heat capacity rate (C_{min}), the temperature of the core-air input to the hydrogen-air heat exchanger determines the amount of heat transfer for a given effectiveness. Therefore, the surface area decreases as the core-air stream is heated from pressurization and the amount of heat transfer is reduced in the air-air heat exchanger (lower right corner). Note that although α_r is quite constant in the hydrogen-air heat exchanger, the size of the finned surface area varies with χ.

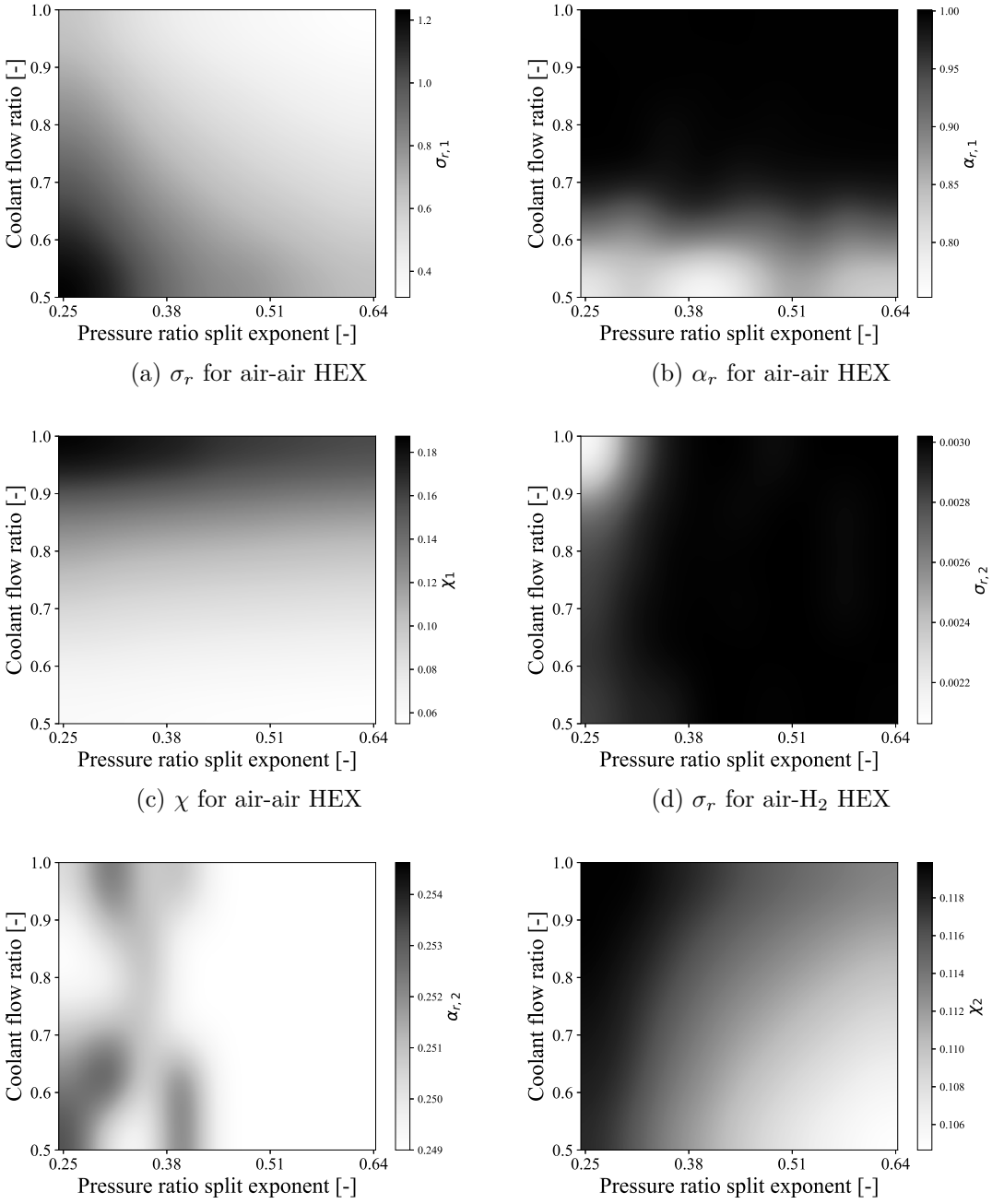

(a) σ_r for air-air HEX

(b) α_r for air-air HEX

(c) χ for air-air HEX

(d) σ_r for air-H_2 HEX

(e) α_r for air-H_2 HEX

(f) χ for air-H_2 HEX

Figure 3.3: Optimal combination of GGPs for the unconstrained design presented in paper 2

3.2 Main contributions

The air-first arrangement in Figure 3.1 corresponds to the intercooler used in the engines shown in Figures 1.9d and 1.3. Although this arrangement seemed like a suitable option prior to the present investigation, there is now data to support those claims. Most other arrangements were excluded on the basis of arguments that should hold throughout the entire design scope of the CCE, but the after-cooled core-air arrangement showed certain benefits, including higher values of fuel heating and reduced risk of freezing. However, the air-first arrangement maintained the main focus during Phase 2, mainly due to the expected benefits that stem from cooling earlier in the core pressurization process. An example case study was conducted where the GenHEX method from Phase 1 was used to estimate the matrix weight and pressure losses for both the core-air to bypass-air and the core-air to hydrogen heat exchangers when coupled in the air-first arrangement. The study was conducted while assuming a fixed volume intercooler, with varying pressure split and coolant flow ratios, and the goal was to achieve 70% effectiveness for the core-air to bypass-air heat exchanger and 95% effectiveness for the core-air to hydrogen heat exchanger. The optimal GGPs for each combination of pressure split and coolant flow ratio are discussed in Section 3.1, highlighting the potential for rapid design space exploration using this novel method and how it can guide the designer in choosing a suitable heat exchanger.

It was also shown that condensation and ice accretion must be taken into account, particularly during low-altitude flight stages. These issues could be mitigated by positioning the heat exchanger further back in the core pressurization process, though a heating element in the fuel stream may be necessary to assist if ice accretion is detected. In addition, hydrogen leakage into the core stream could lead to catastrophic operational failure. To prevent this, a secondary cycle was implemented in which hydrogen transfers heat to a secondary fluid, which in turn transfers heat to the core stream. Helium would be a suitable choice for the fluid to use in the secondary cycle because of the extremely low temperatures required for freezing and the high value of the specific heat capacity. The implementation of the secondary fluid cycle was shown to reduce the overall cooling potential of the intercooler. However, the same heat capacity rate and volume flow as the fuel could be achieved with helium at three times the fuel mass flow and 1.5 times the pressure, resulting in a helium to core-air heat exchanger of similar weight and volume as that for the hydrogen to core-air. Moreover, the secondary cycle also requires an additional hydrogen to helium heat exchanger along with a circulation pump, piping, and manifolds. The impact on performance from adding these additional components is not assessed at this stage, but added risk mitigation may justify the trade-off in such a critical system as an aircraft engine.

Chapter 4

Summary of papers

4.1 Paper 1

In Paper 1, a novel method was presented for the conceptual design of heat exchangers (GenHEX). The GenHEX method facilitates exploration of a continuous design space that spans across heat exchanger families and ultimately gives recommendations for what a suitable heat exchanger should look like for a given application.

4.1.1 Methodology description

The GenHEX method is divided into three parts where the first is a generalized expression of an arbitrary heat exchanger geometry. A detailed explanation of how it was derived is presented in Section 2.1.1 of this thesis. The second part concerns the estimation of the aerothermal performance for the generalized geometry and concludes by presenting correlations for the Colburn factor and Fanning friction factor, an extended discussion on different methods considered is presented in Section 2.1.2 of this thesis. The last part concerns how to establish the traits of a good heat exchanger and concludes that if the method cannot be implemented in a complete system model, an application-specific objective function is required, showing the method how to properly balance between factors such as weight, volume, and pressure losses.

An open source Python-based framework [31] was established in which the novel method was implemented. The results presented for the example case study in Paper 1 were achieved by assessing the performance of heat exchangers that featured a large number of distinct values along each of the three GGPs. Since there were only three open parameters and the computational cost of the method is sufficiently low, no optimization method was required.

4.1.2 Discussion

The generalized expression for the heat exchanger geometry and the method for estimating the aerothermal performance have already been sufficiently discussed in Sections 2.1.1 and 2.1.2. However, the results for the example case study in paper

one are highly dependent on the objective function used for balancing the weight and pressure losses. It is shown how varying the trade offs in the objective function shifts the optimal heat exchanger configuration, further highlighting the importance of providing an accurate objective function if the results are to be deemed useful. Deriving such a function can be challenging without access to a complete system model, and if one is available, the GenHEX model could be integrated straight into that system model instead.

4.2 Paper 2

In Paper 2, the hydrogen-enhanced intercooling concept is introduced and various arrangements are investigated. Selected design considerations including freezing, leakage, and structural integrity are discussed, and methods to establish design constraints are proposed. The GenHEX method introduced in Paper 1 is used for estimating the performance of an unconstrained design and then the change in performance from implementing different risk mitigation methods.

4.2.1 Methodology description

During the first study in Paper 2, the cooling potentials are calculated using the definition of effectiveness, and neither weight, volume nor pressure losses are taken into account. The local cooling power achieved by the intercooler is presented, along with an equivalent cooling power as if achieving the same combustor inlet temperature by cooling just upstream the piston engine inlet. Both the local and equivalent cooling powers provide important information, as the local cooling power is directly related to the heat exchanger design limitations, while the projected cooling power is likely to be an important parameter for engine optimization. The surface temperature and relative humidity at the exit of the hydrogen-air heat exchanger are used to establish a criteria for whether or not freezing will occur. The bulk fluid temperature and cooling power should be chosen in the most critical region of the heat exchanger, which differs depending on whether the heat exchanger operates in counterflow, crossflow, or parallel flow. Methods for inclusion of a secondary cycle are presented, and the impact on overall performance depending on what fluid is chosen and at what mass flow and pressure it operates is shown. During the test case, an iterative sampling optimization method is employed to find which GGPs minimize the objective function. An evenly distributed initial sampling is done; for each iteration, a normal distributed resampling is done around the previous best solution, and the ranges are reduced. This is a rather rapid and robust search method when the computational cost allows for including a large number of configurations.

4.2.2 Discussion

The proposed method for estimating whether freezing will occur is highly limited, since it relies on averaged values of the fluid temperature and cooling power, hence it cannot capture localized freezing. No more accurate method was found that did

not require a detailed analysis of the heat exchanger matrix. However, the chosen method is believed to give an indication for whether detailed studies are required or not.

An improvement of the method for estimating freezing could be to divide the heat exchanger into smaller segments, where each segment would be evaluated separately. This would allow for better capturing effects such as the large variations in specific heat capacity for supercritical parahydrogen, or the reduction in partial pressure of water vapor due to condensation.

Chapter 5

Concluding remarks

5.1 Summary

The task of designing a hydrogen-enhanced intercooler for the composite cycle engine was broken down into 4 different phases, where Phase 1 is considered complete and Phase 2 is ongoing.

Phase 1 resulted in the development of a novel method (GenHEX) that facilitates exploration of the heat exchanger design space in a way that was not possible before. The method guides the designer towards how to design a suitable heat exchanger for a given application, and reduces the demand in designer intuition, luck, and access to extensive databases of heat exchangers. The method was demonstrated and validated by designing an aero engine intercooler as an example case. The estimated performance corresponded well to that of a "state-of-the-art" design.

Phase 2 is still in progress. However, a submitted manuscript is appended to this thesis, in which various arrangements of the hydrogen-enhanced intercooler are compared and a down-selection is made based on cooling potentials achieved using semi-idealized heat exchangers. Various design considerations are discussed, including freezing, leakage, and structural integrity, and methods are proposed to establish design constraints. The GenHEX method developed during Phase 1 is used to estimate the aerothermal performance of a selected arrangement of the hydrogen-enhanced intercooler, along with the impact on performance from various risk mitigation constraints.

Based on the work conducted up to this point, we can reflect back to the objectives and conclude that:

- the GenHEX method facilitates exploration of the heat exchanger design space and allows studies that were cumbersome, or even impossible, before. The method will be used and further developed in the upcoming work.

- there are two main candidates for the arrangement of the hydrogen-enhanced intercooler (the air-first and the after-cooled core air arrangements). Data that could be used in an engine model to represent the intercooler performance are presented.

- the risks associated with using hydrogen as a coolant for intercooling have been discussed and methods have been proposed for constraining the design and thereby mitigating the risks from freezing, leakage, and structural failure. Including the introduction of a secondary cycle with helium.

5.2 Future work

The future work consist of the last two studies required for the main objective, namely how to effectively integrate compact heat exchanger technology into the engine core, and what a suitable intercooler design would look like for the hydrogen-fueled intercooled composite cycle engine. These studies will be conducted in the upcoming phases.

5.2.1 Phase 3: Establishing duct performance charts

During phase 3, the ducts connecting the intercooler to the adjacent compressors and the duct used to extract the bypass air will be investigated. Diffusing ducts are required to reduce the flow velocity of both the core-air stream and the bypass-air stream prior to heat exchanger entry, and a contracting duct will be required to accelerate the flow before entry into the high-pressor compressor. Developing performance charts for the ducts and coupling of those to the GenHEX method would facilitate optimization of the combination of ducts and the intercooler, which could potentially reduce the required engine core length or diameter. However, two key challenges are determined that must be solved for the development of duct performance charts. First, we have to decide for which duct parameters we develop the performance charts. The area ratio along with the ratio of flow turning to duct length are previously used parameters which are non-dimensional and allow for scaling. These two parameters are strong candidates, but others will also be investigated. Second, determining the dependencies between the duct and heat exchanger designs. Varying the heat exchanger design might ease diffusion within the duct, and establishing the performance penalties from having a nonuniform inlet flow to the heat exchanger might ease the demands on the duct design and allow for a shorter overall system. The validation of simulated duct performance will be carried out in the in-house low-speed compressor facility under engine representative conditions.

5.2.2 Phase 4: Integrating the hydrogen-enhanced intercooler into the collaborative MINIMAL engine

During phase 4, surrogate models for estimating the hydrogen-enhanced intercooler, including the adjacent ducts, will be integrated into a complete engine system. This engine will be an intercooled composite cycle engine developed collaboratively in the MINIMAL project and will be optimized for reduced climate impact.

Bibliography

[1] EuropeanParliament. *CO2 emissions from cars: facts and figures (infographics)*. 2019. URL: https://www.europarl.europa.eu/topics/en/article/20190313STO31218/co2-emissions-from-cars-facts-and-figures-infographics (visited on 12/14/2024) (cit. on p. 3).

[2] David S Lee, David W Fahey, Agnieszka Skowron, Myles R Allen, Ulrike Burkhardt, Qi Chen, Sarah J Doherty, Sarah Freeman, Piers M Forster, Jan Fuglestvedt, et al. "The contribution of global aviation to anthropogenic climate forcing for 2000 to 2018". In: *Atmospheric environment* 244 (2021), p. 117834 (cit. on p. 4).

[3] Cordis. *MINIMAL homepage*. 2022. URL: https://cordis.europa.eu/project/id/101056863/results (visited on 12/11/2024) (cit. on p. 4).

[4] Herbert Sammons and Ernest Chatterton. *Napier Nomad Aircraft Diesel Engine*. Tech. rep. 550239. SAE International, 1955. DOI: 10.4271/550239. URL: https://www.sae.org/publications/technical-papers/content/550239/ (cit. on p. 5).

[5] . "Napier Nomad, An Engine of Outstanding Efficiency". In: *Flightglobal* (1954), pp. 543–551 (cit. on p. 5).

[6] Oldmachinepress. *Napier Nomad Compound Aircraft Engine*. 2019. URL: https://oldmachinepress.com/2019/08/05/napier-nomad-compound-aircraft-engine/ (visited on 12/12/2024) (cit. on p. 6).

[7] Cordis. *NEWAC homepage*. 2006. URL: https://cordis.europa.eu/project/id/30876/reporting (visited on 12/12/2024) (cit. on p. 6).

[8] Andrew M Rolt and Nick J Baker. "Intercooled turbofan engine design and technology research in the EU framework 6 NEWAC programme". In: *ISABE 2009 Proceedings, Paper No. ISABE-2009-1278* (2009) (cit. on p. 6).

[9] Günter Wilfert, Joerg Sieber, Andrew Rolt, Nick Baker, Armel Touyeras, and Salvatore Colantuoni. "New environmental friendly aero engine core concepts". In: *ISABE Paper* 2007-1120 (2007) (cit. on p. 6).

[10] Pok-Wang Kwan, David RH Gillespie, Rory D Stieger, and Andrew M Rolt. "Minimising loss in a heat exchanger installation for an intercooled turbofan engine". In: *Turbo Expo: Power for Land, Sea, and Air*. Vol. 54617. 2011, pp. 189–200 (cit. on p. 6).

[11] A Duncan Walker, Jonathan F Carrotte, and Andrew M Rolt. "Duct aerodynamics for intercooled aero gas turbines: constraints, concepts and design methodology". In: *Turbo Expo: Power for Land, Sea, and Air*. Vol. 48883. 2009, pp. 749–758 (cit. on p. 6).

[12] C A'Barrow, JF Carrotte, AD Walker, and AM Rolt. "Aerodynamic performance of a coolant flow off-take downstream of an outlet guide vane". In: *Journal of Turbomachinery* 135.1 (2013), p. 011006 (cit. on p. 6).

[13] Cordis. *LEMCOTECH homepage*. 2011. URL: `https://cordis.europa.eu/project/id/283216/results` (visited on 12/12/2024) (cit. on p. 6).

[14] Xin Zhao, Tomas Grönstedt, and Konstantinos Kyprianidis. "Assessment of the performance potential for a two-pass cross flow intercooler for aero engine applications". In: *International Society for Airbreathing Engines, ISABE, Busan, South Korea, 2013,(ISABE-2013-1215)*. 2013 (cit. on p. 6).

[15] Xin Zhao, Oskar Thulin, and Tomas Grönstedt. "First and second law analysis of intercooled turbofan engine". In: *Journal of Engineering for Gas Turbines and Power* 138.2 (2016), p. 021202 (cit. on p. 6).

[16] Xin Zhao, Mikhail Tokarev, Erwin Adi Hartono, Valery Chernoray, and Tomas Grönstedt. "Experimental validation of the aerodynamic characteristics of an aero-engine intercooler". In: *Journal of Engineering for Gas Turbines and Power* 139.5 (2017), p. 051201 (cit. on pp. 6, 7).

[17] Sascha Kaiser, Arne Seitz, Stefan Donnerhack, and Anders Lundbladh. "Composite cycle engine concept with hectopressure ratio". In: *Journal of Propulsion and Power* 32.6 (2016), pp. 1413–1421 (cit. on p. 7).

[18] Cordis. *ULTIMATE homepage*. 2015. URL: `https://cordis.europa.eu/project/id/633436/reporting` (visited on 12/12/2024) (cit. on p. 7).

[19] Sascha Kaiser, Hagen Kellermann, Markus Nickl, and Arne Seitz. "A composite cycle engine concept for year 2050". In: *Proceedings of the 31st Congress of the International Council of the Aeronautical Sciences, Belo Horizonte, Brazil*. 2018, pp. 9–14 (cit. on p. 7).

[20] Sascha Kaiser, Oliver Schmitz, and Hermann Klingels. "Aero engine concepts beyond 2030: Part 2—the free-piston composite cycle engine". In: *Turbo Expo: Power for Land, Sea, and Air*. Vol. 84140. American Society of Mechanical Engineers. 2020, V005T06A018 (cit. on p. 7).

[21] Sascha Kaiser. "Multidisciplinary Design of Aeronautical Composite Cycle Engines". PhD thesis. Technische Universität München, 2020 (cit. on p. 7).

[22] Bauhaus Luftfahrt. *"Composite Cycle Engine" enables significant fuel burn improvement*. 2019. URL: `https://www.bauhaus-luftfahrt.net/de/topthemen/composite-cycle-engine-enables-significant-fuel-burn-improvement` (visited on 12/14/2024) (cit. on p. 7).

[23] Volker Grewe, Arvind Gangoli Rao, Tomas Grönstedt, Carlos Xisto, Florian Linke, Joris Melkert, Jan Middel, Barbara Ohlenforst, Simon Blakey, Simon Christie, et al. "Evaluating the climate impact of aviation emission scenarios towards the Paris agreement including COVID-19 effects". In: *Nature Communications* 12.1 (2021), p. 3841 (cit. on p. 8).

[24] European Commission. *Communication From the Commission to the European Parliament, the European Council, the Council, the European Economic and Social Committee and the Committee of the Regions-The European Green Deal*. Tech. rep. European Commission Brussels Belgium accessed July 10 2024, 2019 (cit. on p. 8).

[25] Cordis. *ENABLEH2 homepage*. 2018. URL: `https://cordis.europa.eu/project/id/769241/reporting` (visited on 12/12/2024) (cit. on p. 8).

[26] Alexandre Capitao Patrao, Isak Jonsson, and Carlos Xisto. "Compact Heat Exchangers With Curved Fins for Hydrogen Turbofan Intercooling". In: *Journal of Engineering for Gas Turbines and Power* 146.11 (July 2024), p. 111007. ISSN: 0742-4795. DOI: 10.1115/1.4065887. eprint: `https://asmedigitalcollection.asme.org/gasturbinespower/article-pdf/146/11/111007/7353817/gtp\_146\_11\_111007.pdf` (cit. on p. 8).

[27] William Morrow Kays and Alexander Louis London. *Compact heat exchangers*. McGraw-Hill, New York, NY, 1984 (cit. on pp. 13, 15, 17, 21).

[28] David Gordon Wilson and Theodosios Korakianitis. *The design of high-efficiency turbomachinery and gas turbines, with a new preface*. MIT press, 2014 (cit. on p. 13).

[29] Frank P Incropera, David P DeWitt, Theodore L Bergman, Adrienne S Lavine, et al. *Fundamentals of heat and mass transfer*. Vol. 6. Wiley New York, 1996 (cit. on pp. 13, 20).

[30] R.K. Sakhuja P.G. LaHaye F.j. Neugebauer. "A Generalized Prediction of Heat Transfer Surfaces". In: *Journal of Heat Transfer* (1974). DOI: 10.1115/1.3450237 (cit. on pp. 21, 22).

[31] Petter Miltén. *genHEX*. Version 1.0.0. 2024. URL: `https://github.com/PMilten/genHEX` (cit. on p. 31).